Using a magnetometer to image a two-dimensional current distribution

Bradley J. Roth,[a] Nestor G. Sepulveda, and John P. Wikswo, Jr.
Living State Physics Group and Vanderbilt Electromagnetics Laboratory, Department of Physics and Astronomy, Vanderbilt University, Nashville, Tennessee 37235

(Received 16 June 1988; accepted for publication 13 September 1988)

We describe a mathematical algorithm to obtain an image of a two-dimensional current distribution from measurements of its magnetic field. The spatial resolution of this image is determined by the signal-to-noise ratio of the magnetometer data and the distance between the magnetometer and the plane of the current distribution. In many cases, the quality of the image can be improved more by decreasing the current-to-magnetometer distance than by decreasing the noise in the magnetometer.

I. INTRODUCTION

Imaging is a common problem in science and medicine, and many different experimental techniques, such as optical microscopy, x-ray diffraction, and ultrasound, are used to obtain images. In this paper we discuss how to obtain an image of a current distribution by measuring its magnetic field. This imaging technique has biomedical applications, such as noninvasive localization of epileptic spikes in the human brain,[1] and could be used in the electronics industry for nondestructive testing of printed circuit boards, hybrid microcircuits, and large-scale integrated circuits. In biomedical studies, determining a current distribution from a measured magnetic field is called the "biomagnetic inverse problem." We have studied this problem extensively for one-dimensional strands of tissue, such as nerve axons[2] and cardiac muscle,[3] and have applied our one-dimensional analysis to reconstructing current sources in the brain.[4] In this study we generalize our analysis to two-dimensional systems, and stress the relationship between the magnetic inverse problem and other imaging techniques.

The inverse problem, in general, does not have a unique solution. However, for current distributions restricted to two dimensions the inverse problem can be solved uniquely. We solve the inverse problem for a two-dimensional current distribution using the mathematical techniques of Fourier transforms and spatial filtering, which are frequently used in optical imaging. Of central importance to our discussion is the relationship between the signal-to-noise ratio of the measured magnetic field, the distance between the current source and position where the magnetic field is measured, the size of the magnetometer pickup coil, and the spatial resolution of the image of the current distribution.

Figure 1 shows two views of a simulation of a magnetometer signal when the component of the magnetic field normal to a two-dimensional current distribution is measured over a plane 1 mm above the current. Although these data were not measured experimentally, they do represent a possible response of a magnetometer during an experiment, including the presence of noise. A reader with experience in interpreting magnetometer signals may be able to determine by inspection what current distribution gave rise to this magnetic field, but for most readers it is probably difficult to deduce the spatial distribution of current. Our goal is to derive a mathematical algorithm for extracting an image of the current distribution from data such as those presented in Fig. 1.

II. METHODS

A. The forward problem

We assume that a current density $\mathbf{J}(\mathbf{r})$ lies entirely in a thin sheet of thickness d lying in the x-y plane, and that we measure the magnetic field, $\mathbf{B}(\mathbf{r})$, over a plane that is at a height z above the x-y plane, as shown in Fig. 2. The current

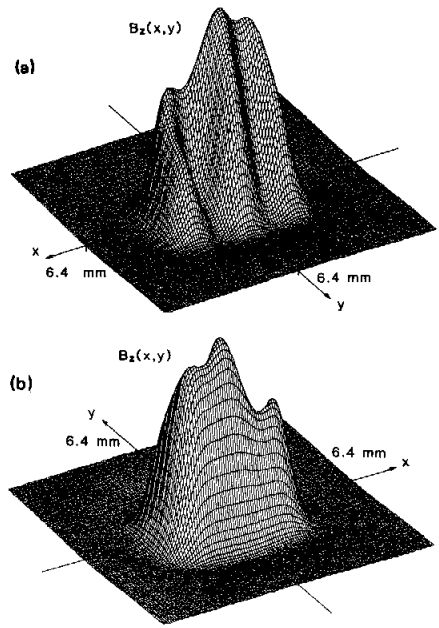

FIG. 1. Two views of simulated magnetometer data. The magnetometer coil, radius 0.35 mm, detected the normal component of the magnetic field, B_z, over a plane 1 mm above a two-dimensional current source. The magnetometer signal has an amplitude of 190 pT and contains 0.5 pT of noise. Our goal is to reconstruct an image of the current distribution that produced this magnetic field.

[a] Present address: Biomedical Engineering and Instrumentation Branch, Division of Research Services, National Institutes of Health, Bethesda, MD 20892.

 0021-8979/89/010361-12$02.40

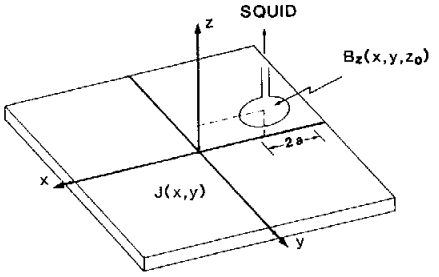

FIG. 2. Schematic diagram of the simulated experiment. The current density, $\mathbf{J}(x,y)$, is restricted to the x-y plane, and the magnetometer measures the z component of the magnetic field, $B_z(x,y,z_0)$, over a plane parallel to the x-y plane, a height z_0 above it. The magnetometer consists of a circular pickup coil, of radius a, attached to a SQUID.

distribution is thin enough that to a good approximation $\mathbf{J}(\mathbf{r})$ can be considered two-dimensional. Furthermore, we assume that the current is quasistatic, so the divergence of the current density vanishes,

$$\nabla\cdot\mathbf{J}=0\,, \tag{1}$$

and we can use magnetostatics to calculate the magnetic field. In this case, the current density and magnetic field are related by the law of Biot and Savart,[5]

$$\mathbf{B}(\mathbf{r})=\frac{\mu_0}{4\pi}\int\frac{\mathbf{J}(\mathbf{r}')\times(\mathbf{r}-\mathbf{r}')}{|\mathbf{r}-\mathbf{r}'|^3}\,d^3\mathbf{r}'\,, \tag{2}$$

where μ_0 is the permeability of free space, $4\pi\times10^{-7}$ T m/A. Let us examine the x component of the magnetic field, B_x. The cross product implies that B_x is produced by the y component of the current density, J_y:

$$B_x(x,y,z)=\frac{\mu_0 d}{4\pi}z\int_{-\infty}^{+\infty}\int_{-\infty}^{+\infty}\frac{J_y(x',y')}{[(x-x')^2+(y-y')^2+z^2]^{3/2}}\times dx'\,dy'. \tag{3}$$

Equation (3) represents a convolution of the current density $J_y(x',y')$ with a weighting function, or Green's function, that depends only on the distance between $\mathbf{r}$ and $\mathbf{r}'$. The convolution theorem[6] allows us to rewrite this equation as

$$b_x(k_x,k_y,z)=g(k_x,k_y,z)j_y(k_x,k_y)\,, \tag{4}$$

where $b_x(k_x,k_y,z)$ and $j_y(k_x,k_y)$ are the two-dimensional Fourier transforms of the magnetic field and current density, respectively, and $g(k_x,k_y,z)$ is the Fourier transform of the Green's function $G(x-x',y-y',z)$:

$$G(x-x',y-y',z)=\frac{\mu_0 d}{4\pi}z\frac{1}{[(x-x')^2+(y-y')^2+z^2]^{3/2}}\,. \tag{5}$$

The two-dimensional Fourier transform is defined as

$$j_y(k_x,k_y)=\int_{-\infty}^{+\infty}\int_{\infty}^{+\infty}J_y(x,y)e^{i(k_x x+k_y y)}dx\,dy, \tag{6}$$

with the inverse Fourier transform given by

$$J_y(x,y)=\frac{1}{(2\pi)^2}\int_{-\infty}^{+\infty}\int_{-\infty}^{+\infty}j_y(k_x,k_y)\times e^{-i(k_x x+k_y y)}dk_x\,dk_y\,. \tag{7}$$

The variables k_x and k_y are the components of the spatial frequency $\mathbf{k}$.

To complete our analysis, we must compute the Fourier transform of the Green's function. The transform of the expression in Eq. (5) can be evaluated analytically[7] and is

$$g(k_x,k_y,z)=(\mu_0 d/2)e^{-\sqrt{k_x^2+k_y^2}\,z}\,. \tag{8}$$

Thus the x component of the magnetic field is just a low-pass-filtered version of the y component of the current density, with the amount of filtering depending on the height above the plane, z.

Similarly, we can calculate the y and z components of the magnetic field:

$$b_y(k_x,k_y,z)=-(\mu_0 d/2)e^{-\sqrt{k_x^2+k_y^2}\,z}j_x(k_x,k_y) \tag{9}$$

and

$$b_z(k_x,k_y,z)=i(\mu_0 d/2)e^{-\sqrt{k_x^2+k_y^2}\,z}\left(\frac{k_y}{\sqrt{k_x^2+k_y^2}}j_x(k_x,k_y)-\frac{k_x}{\sqrt{k_x^2+k_y^2}}j_y(k_x,k_y)\right). \tag{10}$$

We are most interested in the z component of the magnetic field, since this component is often the easiest to measure. From the above equation, it looks as if measuring B_z does not determine both J_x and J_y, but only a linear combination of the two. However, we also know that the current density obeys the equation of continuity, Eq. (1), which in transform space becomes

$$-ik_x j_x(k_x,k_y)-ik_y j_y(k_x,k_y)=0\,. \tag{11}$$

Using this additional relationship between j_x and j_y, it is clear that we obtain both components of the current density by measuring the z component of the magnetic field. In fact, we can obtain both components of the current density from measurements of any one component of the magnetic field.

B. The inverse problem

Our goal is not to calculate the magnetic field from the current density, but just the opposite, to calculate the current density from the magnetic field. One of the great strengths of the spatial filtering technique is that the inverse problem can be solved by merely dividing the magnetic field by the filter to obtain the current density,

$$j_y(k_x,k_y)=\frac{b_x(k_x,k_y,z)}{g(k_x,k_y,z)}\,. \tag{12}$$

This technique works as long as $g(k_x,k_y,z)$ is never equal to zero. However, some filter functions can have zero values. From Eqs. (4), (8), and (11) we find that the relationship between b_x and j_x is

$$j_x(k_x,k_y)=-(2/\mu_0 d)(k_y/k_x)e^{\sqrt{k_x^2+k_y^2}\,z}b_x(k_x,k_y,z). \tag{13}$$

When k_x is zero, the inverse filter function goes to infinity. This is equivalent to saying that a uniform current in the x direction does not produce an x component of the magnetic field. Thus, the calculation does not have a unique solution, to the extent that measurements of B_x or B_z cannot detect a uniform current in the x direction, and similarly, measurements of B_y and B_z cannot provide information about uniform currents in the y direction (although measurements of both B_x and B_y do uniquely specify the current distribution). The inverse filter function also goes to infinity as $\sqrt{k_x^2+k_y^2}$ approaches infinity. This behavior does not present a problem as long as the spatial frequency spectrum of the magnetic field is band-limited. The exponential increase in the inverse filter implies that the computed current density is a high-pass-filtered version of the magnetic field.

Spatial frequency analysis, like that presented here, is used extensively in optical imaging, and many of the concepts used in Fourier optics can be applied to the magnetic inverse problem. However, a fundamental difference between the two imaging techniques is that optical imaging involves electromagnetic waves that have both amplitude and phase, while the magnetic field we measure is not a wave and therefore has no phase. Therefore, optical imaging techniques that depend on interference phenomena do not have obvious analogies in the magnetic inverse problem. Image restoration techniques developed for optical studies[8] may improve our current images. These techniques use *a priori* knowledge about the current density, for example, the fact that a current distribution may be localized on a 5×5-mm^2 silicon chip, to improve the image quality.

C. Numerical implementation of the calculation

To implement this calculation on a digital computer, we must consider fields sampled at a finite number of discrete points instead of continuous functions defined over the entire x-y or k_x-k_y plane. Since discrete frequency spectra arise when considering periodic functions, we assume that the current density is periodic with periods X and Y in the x and y directions. Although in experiments we do not study periodic currents, we can select X and Y sufficiently large that our assumption of periodicity does not affect significantly our results. In practice, X and Y must be selected much larger than both the spatial dimensions of the current source and the height of the magnetometer above the x-y plane. We sample the current density at discrete points, where N_x and N_y are the number of points along each axis of a rectangular grid with sides of length X and Y, and Δx and Δy are the distances between adjacent points in the grid ($\Delta x = X/N_x$ and $\Delta y = Y/N_y$). The distances between points in the k_x-k_y plane are Δk_x and Δk_y, where $\Delta k_x = 2\pi/(N_x \Delta x)$ and $\Delta k_y = 2\pi/(N_y \Delta y)$. If the frequency spectrum of the current density is band-limited, and if the maximum spatial frequencies contributing to the current, K_x and K_y, are less than $\pi/\Delta x$ and $\pi/\Delta y$, respectively, then by the Whittaker–Shannon sampling theorem the continuous current density can be completely recovered from the sampled data.[9] If the fields are not band-limited, then aliasing errors may be present in the discrete representation of the field.

To avoid aliasing errors in our simulations, we do not consider currents confined to infinitesimally thin wires, but instead study only smooth current distributions produced by convolving the current density in a wire loop with a Gaussian, $e^{-r^2/\lambda^2}/\lambda^2\pi$, where the length constant λ determines the amount of smoothing. Convolution by this Gaussian in the x-y plane is equivalent to multiplication by $e^{-k^2\lambda^2/4}$ in the frequency plane. Although the frequency spectrum of such a current density is not strictly band-limited, the Gaussian greatly attenuates the spatial frequency content of the current distribution at large k, minimizing aliasing errors.

D. Experimental considerations

When making experimental measurements of the magnetic field, we must consider the size of the pickup coil used in the magnetometer and the presence of noise in the data. We assume that these experiments use a superconducting quantum interference device (SQUID) to detect the current in a square or circular pickup coil, and that the coil is oriented so that it is sensitive to only the z component of the magnetic field (Fig. 2). Spatial frequency techniques have been used to analyze gradiometers (magnetometers containing several pickup coils at different positions), where they assume that each pickup coil has negligible area.[10] Here, we use spatial frequency methods to analyze the response of a single pickup coil with a finite area.

It is not the magnetic field at a point but instead the field averaged over the coil area that determines the signal measured by the SQUID. This averaging process is equivalent to a convolution of the magnetic field with a step function $H(\mathbf{r})$, which is

$$H(r) = \begin{cases} 1/(\pi a^2), & r<a \\ 0, & r>a \end{cases} \tag{14}$$

for a circular pickup coil of radius a, and

$$H(x,y) = \begin{cases} 1/L^2, & |x|<L/2 \text{ and } |y|<L/2 \\ 0, & |x|>L/2 \text{ or } |y|>L/2 \end{cases} \tag{15}$$

for a square coil with sides of length L. Using the convolution theorem, we can account for the area of the pickup coil by multiplying the Fourier transform of the magnetic field by the Fourier transform of the step function, $h(\mathbf{k})$, which for the circular loop is

$$h(k,\phi) = \frac{J_1(ka)}{ka/2}, \tag{16}$$

where J_1 is the Bessel function of the first kind and first order, and for the square loop is

$$h(k_x,k_y) = \frac{\sin(k_xL/2)}{k_xL/2}\,\frac{\sin(k_yL/2)}{k_yL/2}. \tag{17}$$

These functions are plotted in Fig. 3. When solving the inverse problem, the Fourier transform of the measured magnetic field must be divided by $h(\mathbf{k})$ before calculating the current density. A difficulty arises because both of these functions have zeros in the k_x-k_y plane. If a or L is small enough that the first zero of $h(\mathbf{k})$ lies outside the largest frequency contributing to the spatial frequency spectrum of the current density image, the difficulty is avoided. Thus for a square pickup coil the largest frequency contributing to the current image, $k_{\max}$, must be less than $2\pi/L$, and for a circu-

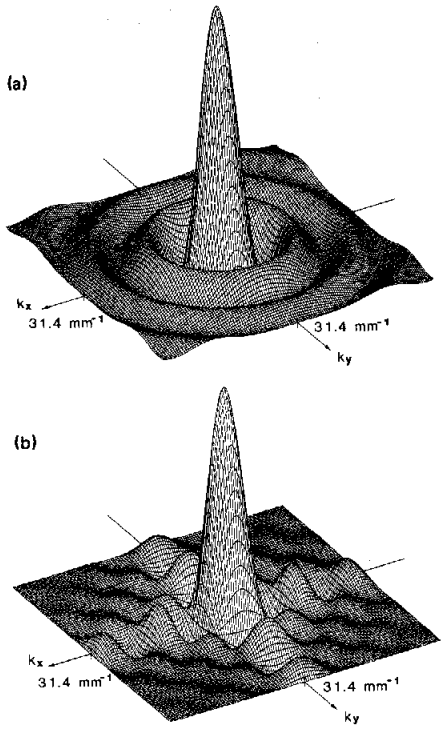

FIG. 3. Filter functions in spatial frequency space corresponding to the averaging of the magnetic field over (a) a circular pickup coil with a radius $a = 0.564$ mm, Eq. (16), or (b) a square pickup coil with sides of length $L = 1$ mm, Eq. (17). Both filter functions have a peak amplitude of 1. The radius of the circular coil was selected so that the two coils have equal areas. The first zero of the filter function in (a) occurs at $3.83/a$, and in (b) at $2\pi/L$.

lar coil, k_{max} must be less than $3.83/a$, where 3.83 is the first zero of $J_1(x)$.[11] If k_{max} is larger than these values, then some spatial frequencies will not be recoverable from the measured data, and the inverse problem cannot be solved uniquely.

Noise is present in any experimental measurement. We assume that environmental noise is eliminated by shielding. The amount of noise in a SQUID system varies widely, but a typical SQUID magnetometer has an intrinsic noise of 15 to 50 fT/$\sqrt{\text{Hz}}$. If the SQUID is operated with a temporal bandwidth of 100 Hz, typical of biomedical applications,[12] the resulting signals have a maximum noise of 0.5 pT. We assume that the magnetometer noise is evenly distributed over all spatial frequencies.

The presence of noise has important ramifications for solving the inverse problem. The frequency spectrum of the measured magnetic field will be dominated by noise at high spatial frequencies, and when we calculate the current density from the magnetic field we amplify these high-frequency components. Thus, in the presence of noise, the inverse calculation is unstable because we inevitably amplify high-frequency noise. To surmount this difficulty, we must low-pass filter our measured magnetic field to eliminate the high-spatial-frequency components before computing the current density. We do this by multiplying the magnetic field in frequency space by a Hanning window,[13]

$$W(k) = \begin{cases} 0.5[1 + \cos(\pi k / k_{max})], & k < k_{max} \\ 0, & k > k_{max} \end{cases} . \quad (18)$$

The cutoff frequency, k_{max}, must be determined empirically and is affected by the amplitude of the magnetometer noise, the spatial frequency content of the current distribution, the size of the magnetometer pickup coil, and the height z of the magnetometer above the x-y plane. The attenuation of the high-spatial-frequency components of the magnetic field results in a loss of spatial resolution in the calculated current distribution. Thus, the noise in the measurement limits the spatial resolution of the image.

We would like to have some quantitative estimate of the quality of an image. One figure of merit is the normalized mean-square deviation (MSD) between the original current density, $\mathbf{J}(x,y)$, and its image, $\mathbf{J}_{image}(x,y)$:

$$\text{MSD} = \frac{\int_{-\infty}^{+\infty}\int_{-\infty}^{+\infty} |\mathbf{J}(x,y) - \mathbf{J}_{image}(x,y)|^2 \, dx \, dy}{\int_{-\infty}^{+\infty}\int_{-\infty}^{+\infty} |\mathbf{J}(x,y)|^2 \, dx \, dy} . \quad (19)$$

The parameter measures both the amplitude of the background noise and the loss of spatial resolution. The smaller the MSD, the better the image; if the MSD is zero, the current density and its image are identical. The MSD is not the only way to compare the image quality. In fact, selecting a single criterion as the definition of "quality" is arbitrary. However, this parameter does allow us to compare the images and say something about their relative quality.

III. RESULTS

In this section we analyze quantitatively the relationship between noise, the source-to-field point distance, coil size, and spatial resolution for a specific current distribution. Figure 4 outlines our calculation. We start with a known current density, solve the forward problem of calculating the magnetic field, add noise, solve the inverse problem of calculating an image of the current density, and then compare the original current density with its image. In the following calculations we use a grid containing 128 points in the x and y directions, with a distance between points of 0.1 mm.

Figure 5(a) shows the current lines produced by a square current loop with sides of 1 mm, carrying 1 μA of current, convolved with a Gaussian of length constant $\lambda = 0.15$ mm to satisfy the sampling theorem. The x component of this current density, $J_x(x,y)$, is plotted in Fig. 6(a), and the imaginary part of its Fourier transform, $j_x(k_x,k_y)$, is shown in Fig. 6(b) (for this particular example, j_x is pure imaginary). The amplitude of the current density is proportional to the total current around the loop and is inversely proportional to the thickness of the sheet containing the current distribution, d; for this example we assume d is 1 μm (the only effect d has on our calculation is to change the amplitude of the current density, the magnetic field does not depend on d). The Fourier transform of the z component of the magnetic field, $b_z(k_x,k_y)$, is calculated from Eqs. (10) and (11), and the real part of b_z calculated 1 mm above the x-y plane is shown in Fig. 6(c). Note that the exponential

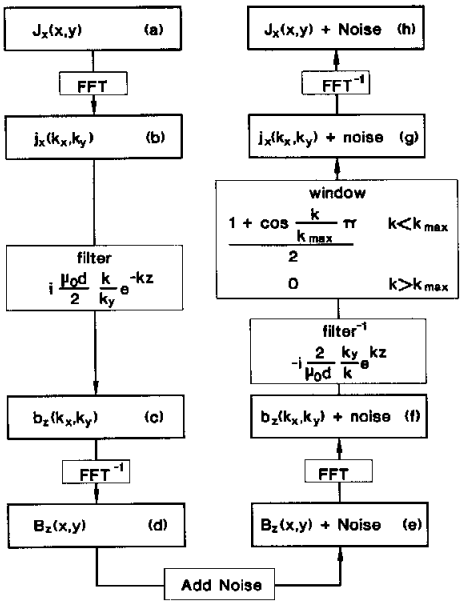

FIG. 4. Schematic diagram summarizing the forward and inverse problems. Starting with a known x component of the current density, $J_x(x,y)$, we calculate the z component of the magnetic field, $B_z(x,y,z)$, then add noise, and calculate an image of the current density from the noisy magnetic field.

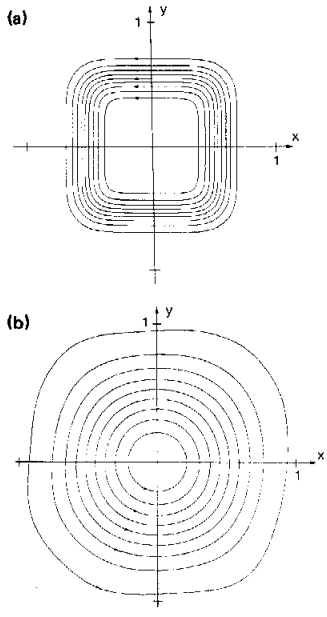

FIG. 5. (a) Square current loop with 1-mm-long sides carrying 1 μA. The current distribution across the loop cross section is Gaussian, with length constant $\lambda = 0.15$ mm. Each line corresponds to a current of 0.1 μA. The arrows indicate the direction of the current density at each point, and the density (spacing) of the lines indicates the amplitude of the current density. (b) The image of the current loop in (a), obtained from the magnetic field with noise; $z = 1$ mm, noise = 0.5 pT, $k_{max} = 10\ mm^{-1}$.

e^{-kz} in the filter function causes high spatial frequencies in j_x to be greatly attenuated in b_z. The inverse Fourier transform yields the magnetic field as a function of x and y, shown in Fig. 6(d), which would be measured by a magnetometer in the absence of noise.

To determine how the magnetometer noise affects our calculation, we add spatially white noise with an amplitude of 0.5 pT to the magnetic field, as shown in Fig. 6(e). From the Fourier transform of this signal, Fig. 6(f), we see that at low spatial frequencies the signal dominates the noise, but above $k \approx 10\ mm^{-1}$ the noise is larger than the signal. When we perform the inverse calculation using this magnetic field, we find that because of the exponential factor e^{kz} in the inverse filter function only the highest-frequency components contribute to the current density image, where noise completely dominates the magnetic field. Therefore, we low-pass filter our current-density image using the Hanning window, selecting k_{max} to be the spatial frequency where the contribution of signal and noise are approximately equal, $k_{max} = 10\ mm^{-1}$. The windowed Fourier transform of the current density is shown in Fig. 6(g), where the circle has a radius of k_{max} and all frequency components at spatial frequencies larger than k_{max} vanish. When we perform the inverse Fourier transform, we obtain the x component of the current density shown in Fig. 6(h), which can be compared to Fig. 6(a). There are two differences between the current and its image. First, in Fig. 6(h) there is some low-amplitude noise throughout the x-y plane. Second, the current distribution has been widened, rounded, and has a smaller amplitude; we have lost spatial resolution. These same conclusions can be seen in Fig. 5(b), where a plot of the current lines for the current-density image is presented (the line-follower algorithm we used was unable to plot the many small current loops resulting from the noise).

Figure 5 illustrates that in the presence of noise we do not obtain a perfect image of the current density from measurements of the magnetic field. Our goal, then, is to obtain the best possible image. There are three primary factors that determine the spatial resolution: our choice of the cutoff frequency of our low-pass filter, k_{max}; the height of the magnetometer above the current distribution, z; and the amount of noise in the measured magnetic signal. Our choice of k_{max} is somewhat arbitrary. We could choose k_{max} larger, thereby increasing the spatial resolution of our image, but also increasing the background noise. Conversely, we could eliminate much of the noise by selecting a smaller value for k_{max}, with an accompanying rounding of our calculated current. Figure 7 shows the calculated current density for three values of k_{max} (8, 10, and 12 mm^{-1}). At $k_{max} = 12\ mm^{-1}$ the signal-to-noise ratio of the image is very poor, and if k_{max} is taken much larger the signal will be lost in the noise; i.e., the calculation is unstable. The image calculated with $k_{max} = 10\ mm^{-1}$ has the smallest mean-square deviation, indicating that, at least by one criterion, in Fig. 7, part (b) is the highest-quality image.

The height of the magnetometer above the current distribution is particularly important for determining the spatial resolution of our calculated current. In Fig. 8 we repeat the calculation performed in Fig. 6, but for $z = 0.3$ mm in-

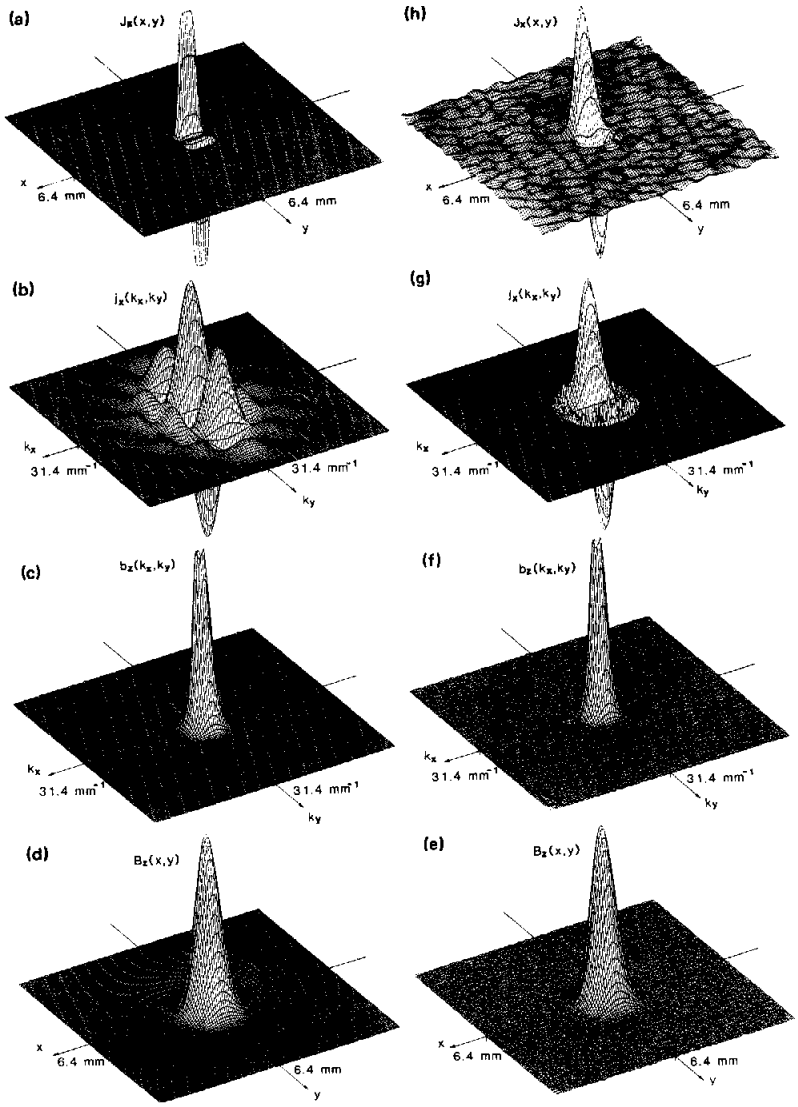

FIG. 6. Forward and inverse calculations for $z = 1$ mm. (a) The x component of the current density, $J_x(x,y)$, for the same current loop as in Fig. 5(a), with peak amplitude of 3.76 mA mm^{-2}, (b) the imaginary part of the Fourier transform of the x component of the current density, $j_x(k_x,k_y)$, (c) the real part of the Fourier transform of the z component of the magnetic field, $b_z(k_x,k_y)$, at $z = 1$ mm, and (d) the z component of the magnetic field, $B_z(x,y)$, with peak amplitude of 126 pT. (e) The same z component of the magnetic field as in (d), but with 0.5-pT amplitude noise added, (f) the real part of the Fourier transform of the z component of the magnetic field with added noise, (g) the imaginary part of the Fourier transform of the x component of the current-density image, multiplied by, a Hanning window, Eq. (18), with $k_{max} = 10\ mm^{-1}$, and (h) the x component of the current density image, with peak amplitude of 1.42 mA mm^{-2}.

stead of 1 mm. Note that for the smaller value of z, there is much more high-frequency information in the magnetic signal. The signal-to-noise ratio of the magnetic field at $z = 0.3$ mm is better than that at $z = 1.0$ mm for two reasons: The amplitude of the signal is larger since the magnetometer is closer to the source, and the high-frequency information in the signal has not been attenuated as severely. Thus, we can select k_{max} to be larger than that in Fig. 6, taking $k_{max} = 30\ mm^{-1}$, as evidenced by the larger circle of non-zero field in Fig. 8(g). Since there is essentially no contribution to the frequency spectrum of the current density at such high spatial frequencies, we recover the original current density without distortion and with little noise. In Fig. 9 and Table I we compare the calculated current density using four different values of z: 0.1, 0.3, 1.0, and 3.0 mm. At $z = 0.1$ mm, the current can be recovered with the correct amplitude and little distortion. But at $z = 3$ mm, the image of the current density is extremely rounded and bears little resem-

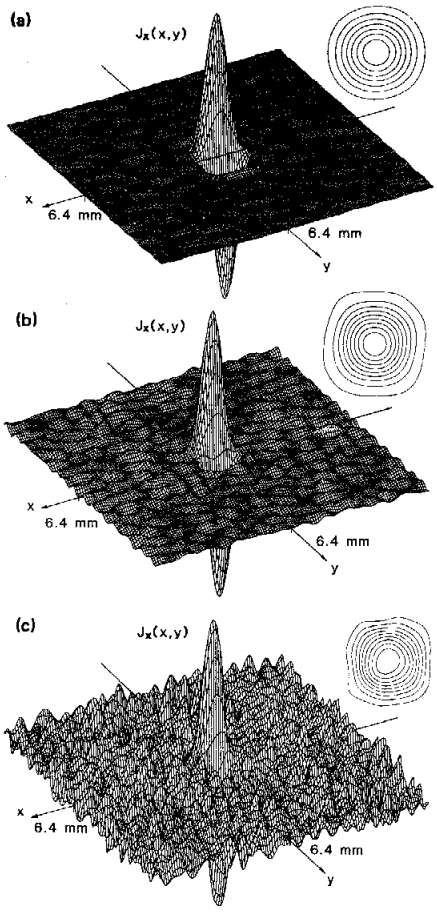

FIG. 7. Image of the current density for three different values of k_{max}. Both a plot of $J_x(x,y)$ and the current lines (upper right inset) are shown. The current density image is calculated from the z component of the magnetic field at $z = 1$ mm produced by the square current loop shown in Fig. 5, where magnetometer noise with an amplitude of 0.5 pT has been added to the magnetic field. A Hanning window, Eq. (18), with cutoff frequency k_{max}, was used for the inverse calculation. The amplitude of the x component of the current density image, J_x^{max}, and the mean square deviation (MSD) are tabulated below:

	k_{max} (mm^{-1})	J_x^{max}(mA mm^{-2})	MSD
(a)	8	1.08	0.52
(b)	10	1.42	0.44
(c)	12	1.78	0.64

blance to the original current density. Moreover, the total current predicted in the loop is 0.19 μA, underestimated by more than a factor of 5. It is clear that to obtain an accurate image of the current density from measurements of the magnetic field, the magnetometer must be close to the source. As a rule of thumb, the distance from the magnetometer coil to the source, z, should be as small or smaller than the characteristic scale length of the current source. In our case, the current distribution has two characteristic lengths: each side of the current loop is 1-mm long, and the width of each side is on the order of 0.15 mm. The 0.15-mm width is evident at spacings of 0.3 mm or less; the 1-mm diameter of the loop is lost at a 3-mm spacing.

One aspect of the current distribution is correctly predicted by each image in Fig. 9. The dipole moment $\mathbf{m}$ is defined as $1/2\mathbf{r}\times\mathbf{J}$ integrated over the volume of the current distribution.[14] This definition is equivalent to saying that the dipole moment strength m is equal to the current strength times the area of the current in loop. In our case, the loop carries 1 μA and has an area of 1 mm^2, so $m = 1\ \mu$A mm^2. To a high accuracy, this value is correctly predicted from each current image in Fig. 9; the largest error in predicting the dipole moment is 7% at $z = 1$ mm, apparently due to the noise. Thus we see that calculations of the dipole moment of a current distribution (in μA mm^2) from measurements of the magnetic field may be quite accurate. But to determine individually the spatial size (in mm) and current strength (in μA) of a current distribution, an analysis such as ours must be used, and it is essential that the source-to-measuring distance be reduced as much as possible.

The third factor in determining the best possible spatial resolution is the amplitude of the noise in the magnetometer. However, if the measurement is made at large z, a decrease in noise makes a surprisingly small improvement in the calculated image of the current. Let us compare two magnetometers, one capable of being positioned only within 3 mm of the current source, and a second capable of being positioned within 1 mm. Furthermore, we make the somewhat unrealistic assumption that, because of technical reasons in the design of magnetometers, the magnetometer that can be placed 1 mm from the source has 100 times the noise present in the other magnetometer. In other words, the designer of the second magnetometer traded a factor of 100 increase in noise for a factor of 3 in source-to-coil distance. Which magnetometer provides the best image of the current distribution? Figure 10 shows the magnetic field and calculated image of the current density in these two cases. The quality of the images are nearly identical (MSD = 0.947). We conclude that as long as the coil-to-current spacing is comparable to or larger than the characteristic scale length of the current source, improvement in the quality of the reconstructed current density is more sensitive to the coil-to-source distance than to the amount of noise in the magnetometer. If z is small, or if there is excessive noise in the magnetometer so that the signal-to-noise ratio is less than 1, then reducing the noise in the signal becomes increasingly important. Nevertheless, in many applications of SQUID magnetometry, dramatic increases in the spatial resolution of the imaged current might be obtained by decreasing the source-to-coil distance.

The magnetometer pickup coil size also plays a role in determining the quality of the image. Figure 11 shows, for two coil radii, the z component of the magnetic field, with noise, measured 1 mm above the plane of the current, and the reconstructed image of the current density, using $k_{max} = 10$ mm^{-1}. In Fig. 11(a) the magnetic field is calculated for the limiting case of a coil with zero radius, while in Fig. 11(c) the field is averaged over a circular coil with a 0.35-mm radius. This radius is small enough that the first

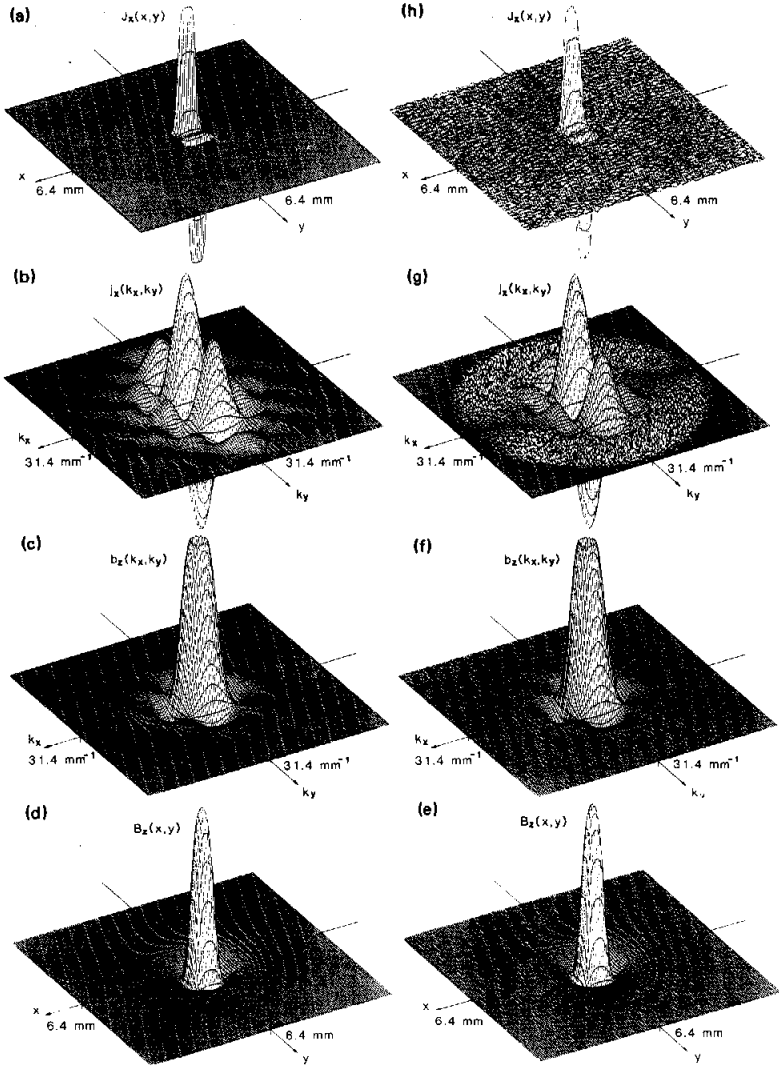

FIG. 8. Forward and inverse calculations for $z = 0.3$ mm. (a) The x component of the current density, $J_x(x,y)$, for the same current loop as in Fig. 5(a), with peak amplitude of 3.76 mA mm^{-2}, (b) the imaginary part of the Fourier transform of the x component of the current density, $j_x(k_x,k_y)$, (c) the real part of the Fourier transform of the z component of the magnetic field, $b_z(k_x,k_y)$, at $z = 0.3$ mm, and (d) the z component of the magnetic field, $B_z(x,y)$, with peak amplitude of 756 pT. (e) The same z component of the magnetic field as in (d), but with 0.5-pT amplitude noise added, (f) the real part of the Fourier transform of the z component of the magnetic field with added noise, (g) the imaginary part of the Fourier transform of the x component of the current-density image, multiplied by a Hanning window, Eq. (18), with $k_{max} = 30$ mm^{-1}, and (h) the x component of the current-density image, with peak amplitude of 3.08 mA mm^{-2}.

zero in the coil inverse filter function is greater than k_{max}, so a unique solution to the inverse problem exists. Although a coil of this size changes the shape of the magnetic field only slightly, it does reduce the quality of the current image.

IV. EXTENSIONS TO THREE-DIMENSIONAL CURRENT DISTRIBUTIONS

For two-dimensional current distributions, the magnetic inverse problem—solving the current distribution from the magnetic field—has a unique solution; in three dimensions it does not. This presents a fundamental limitation to our ability to predict current distributions from magnetic measurements. We can generalize our previous results by considering a current distribution of non-negligible thickness. Specifically, consider a current distribution contained in an unbounded slab of thickness d, with the surfaces of the slab at $z = \pm d/2$. The current density now has three components, and the equation of continuity becomes

$$-ik_x j_x(k_x,k_y,z) - ik_y j_y(k_x,k_y,z) + \frac{\partial j_z(k_x,k_y,z)}{\partial z} = 0 . \tag{20}$$

The z component of the magnetic field produced by this current density is

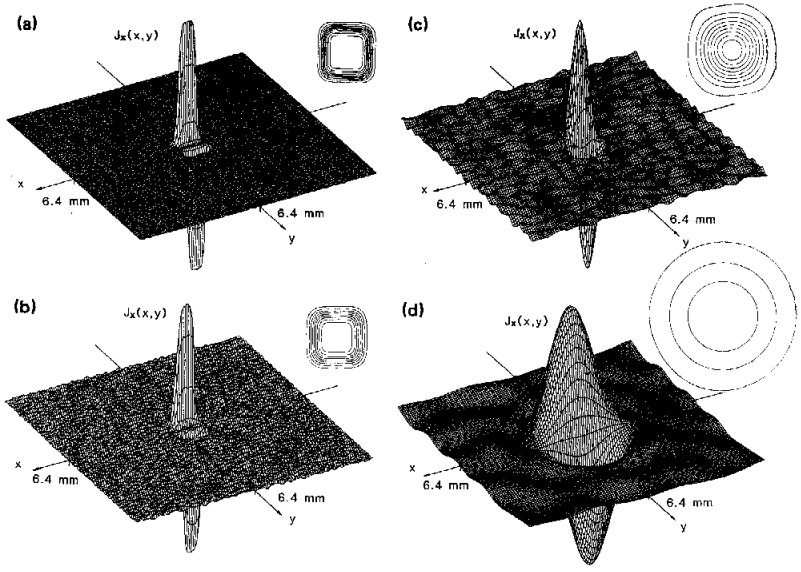

FIG. 9. Image of the current density for four different values of z, calculated from the z component of the magnetic field produced by the square current loop shown in Fig. 5 after magnetometer noise of 0.5 pT has been added to the magnetic field. Plots of both $J_x(x,y)$ and the current lines (upper right inset) are shown. Each line corresponds to 0.1 μA, except in (d), where each line is 0.05 μA. The peak amplitude of the current density, $J_x^{\max}$, the total current in the loop, I, the dipole moment m, and the mean square deviation MSD are listed in Table I.

$$B_z(x,y,z)=\frac{\mu_0}{4\pi}\int_{-d/2}^{+d/2}\int_{-\infty}^{+\infty}\int_{-\infty}^{+\infty}\frac{(y-y')J_x(x',y',z')-(x-x')J_y(x',y',z')}{[(x-x')^2+(y-y')^2+(z-z')^2]^{3/2}}\,dx'\,dy'\,dz'\,. \tag{21}$$

Using the convolution theorem, this equation becomes

$$b_z(k_x,k_y,z)=\int_{-d/2}^{+d/2}\left[i\frac{\mu_0}{2}e^{-\sqrt{k_x^2+k_y^2}(z-z')}\times\left(\frac{k_y}{\sqrt{k_x^2+k_y^2}}j_x(k_x,k_y,z')-\frac{k_x}{\sqrt{k_x^2+k_y^2}}j_y(k_x,k_y,z')\right)\right]dz'\,. \tag{22}$$

Note that we cannot solve for $j_x(k_x,k_y,z')$ or $j_y(k_x,k_y,z')$ themselves, but only their integrals over z'. In other words, from our measurements of the magnetic field we cannot tell the difference between localized (high spatial frequency) deep ($z-z'$ large) currents and diffuse (low spatial frequency) shallow ($z-z'$ small) currents. This is a fundamental limitation, and in general cannot be overcome without making invasive measurements of the magnetic field inside the slab ($-d/2<z<d/2$).

How much information can we obtain from noninvasive magnetic measurements? The magnetic signals are difficult to interpret for two reasons. First, there is the unsolvable problem of the nonuniqueness of the current-density image. Second, the field point distance z may be large enough that the magnetic field has been severely low-pass filtered, a limitation that is also present in measurements of two-dimensional current sources and was discussed in detail previously. We can minimize the filtering problem if our data have a good signal-to-noise ratio. The magnetic field everywhere outside the source region (above the slab) can be calculated from measurements over any one surface for which z is a constant. In particular, we can make our measurements at z_1, and then determine uniquely the magnetic field at another plane, z_2. The location of z_2 could be anywhere above the slab, including at the slab surface, $z_2=d/2$. We call this calculation the inward continuation of the magnetic field. We cannot determine the magnetic field inside the slab, for then we encounter the nonuniqueness problem. But we can compute the magnetic field at the surface of the slab and thereby put back many of the high spatial frequencies.

The inward continuation is trivial in the spatial frequency domain. The z component of the magnetic field at z_2, $b_z(k_x,k_y,z_2)$, can be related to the measured z component of the magnetic field, $b_z(k_x,k_y,z_1)$, at a distance z_1 by

TABLE I. Image quality for different values of z.

	z (mm)	$k_{\max}$ (mm^{-1})	$J_x^{\max}$ (mA mm^{-2})	I (μA)	m (μA mm^2)	MSD
(a)	0.1	100	3.77	1.00	0.99	0.03
(b)	0.3	30	3.08	1.00	0.99	0.07
(c)	1.0	10	1.42	0.93	1.07	0.44
(d)	3.0	3	0.13	0.19	0.99	0.95

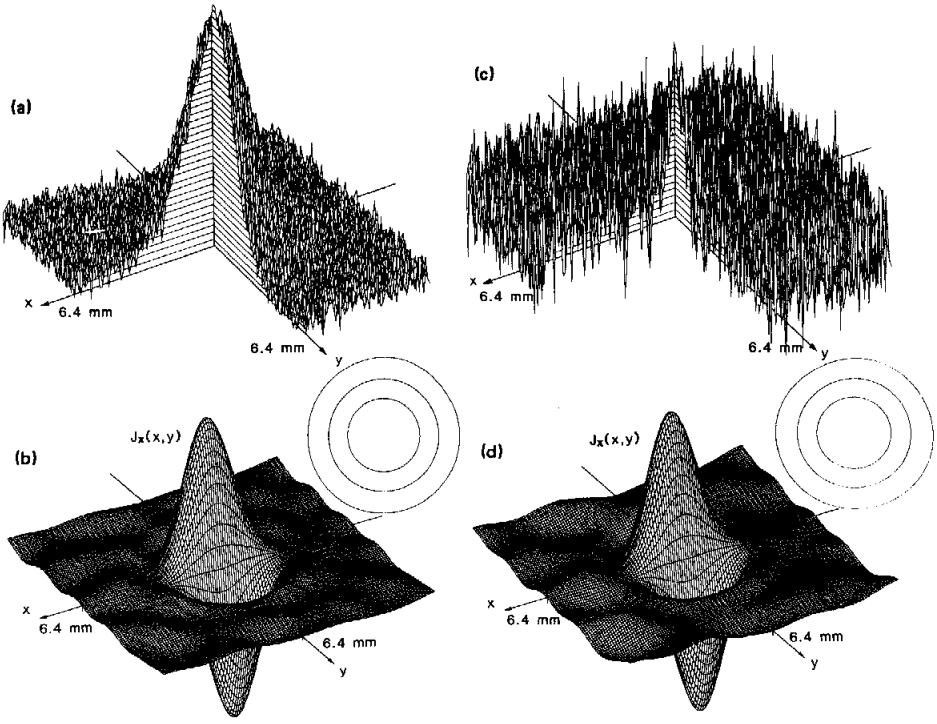

FIG. 10. Magnetic field and the image of the current density for two different values of magnetometer noise and two different magnetometer distances. The current density is calculated from the z component of the magnetic field produced by the square current loop in Fig. 5(a). Plots of both $J_x(x,y)$ and the current lines (upper right inset) are shown. In the plots of the magnetic field, the first quadrant is not shown so the signal can more easily be distinguished from the noise. (a) Magnetic field, 6.5 pT, and (b) image of the current density, 0.13 mA mm^{-2}, for a low-noise magnetometer 3 mm from the current. (c) Magnetic field, 126 pT, and (d) image of the current density, 0.13 mA mm^{-2}, for a noisy magnetometer 1 mm from the current:

	z (mm)	noise (pT)	k_{max} (mm^{-1})	MSD
(a) and (b)	3.0	0.5	3.0	0.947
(c) and (d)	1.0	50.0	3.0	0.947

$$b_z(k_x,k_y,z_2) = e^{\sqrt{k_x^2+k_y^2}(z_1-z_2)} b_z(k_x,k_y,z_1). \qquad (23)$$

Clearly when z_2 is less than z_1 the exponential term acts like a high-pass filter, amplifying the high-spatial-frequency components of the signal. The inward continuation provides as much information as possible from the magnetic measurements without making any assumptions about the current distribution, i.e., the inward continuation is not dependent on a specific source model.

Once the magnetic field has been measured over one plane of constant z, additional information cannot be gained by measuring the magnetic field over additional planes at different heights, since we can uniquely calculate the magnetic field at one value of z from the magnetic field at another z using the inward continuation. Also, we cannot get additional information by measuring more than one component of the magnetic field, since in the region above the current distribution both the divergence and the curl of the magnetic field vanish, providing enough constraints that one field component suffices to specify the magnetic field completely (except for a current density that is uniform in the x or y direction). To gain more information requires us to make an assumption about the current density, i.e., to replace the general current distribution with one constrained by a model.

Let us consider a special case for the current density, in which the source is known to consist of two parallel slabs separated by a distance e, each of negligible thickness d and containing unknown two-dimensional current distributions, $\mathbf{J}(x,y,+e/2)$ and $\mathbf{J}(x,y,-e/2)$. We cannot obtain the current density in both slabs by measuring the magnetic field above the upper slab. Now let us further assume that this current distribution is such that we can measure the magnetic field both above and below the slabs, i.e., we can measure B_z at $z>e/2$ and at $z<-e/2$, for example, by flipping the source over. Then we can obtain two equations that are linearly independent and can therefore solve for both of the current densities. However, if the current densities are coupled, so that current can pass from the upper to the lower slab, then we can no longer obtain a unique solution.

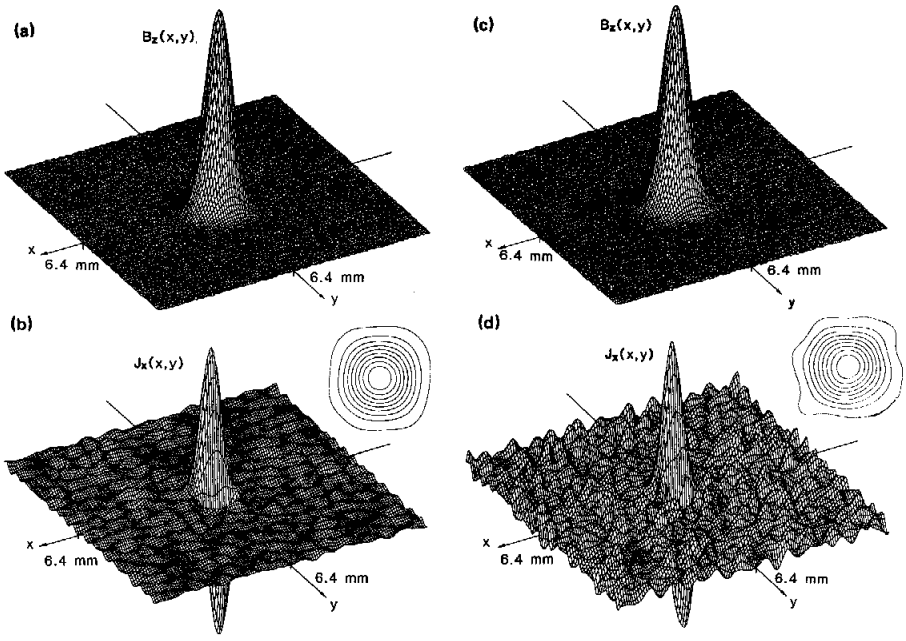

FIG. 11. Magnetic field and the current-density image calculated using two sizes of magnetometer pickup coils. (a) Magnetic field measured with a negligibly small coil radius, $z = 1$ mm, noise $= 0.5$ pT, and (b) the current image, $k_{max} = 10\ \text{mm}^{-1}$, MSD $= 0.43$. Both a plot of $J_x(x,y)$ and the current lines (upper right inset) are shown. The same (c) magnetic field, and (d) current image, except that the magnetometer pickup coil had a radius of 0.35 mm, MSD $= 0.54$.

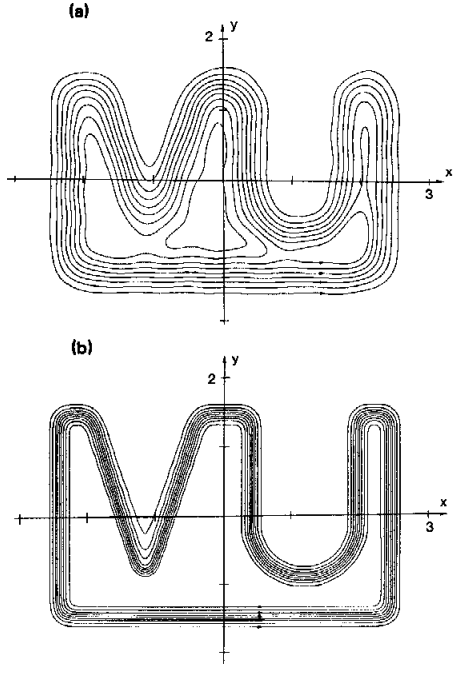

FIG. 12. (a) Image of the current density, calculated from the noisy magnetic field in Fig. 1: $z = 1.0$ mm, $k_{max} = 10\ \text{mm}^{-1}$, noise $= 0.5$ pT, $a = 0.35$ mm, and MSD $= 0.40$. (b) Current density used to calculate the magnetic field in Fig. 1. The loop carries 1 μA of current, and the current profile across the loop cross section is Gaussian, with $\lambda = 0.15$ mm.

Recently, Dallas[15] has outlined a technique for three-dimensional reconstruction of electrical currents in the human brain from noninvasive measurements of the magnetic field. He uses the Fourier-transformed Maxwell's equations and the Whittaker–Shannon sampling theorem to solve the inverse problem. It is not clear how his technique handles the nonuniqueness of the calculated current density. Dallas acknowledges that the current image may not be unique, but does not explain the implications of nonuniqueness on his reconstruction algorithm. Kullmann and Dallas[16] used this technique to image currents, but only considered two-dimensional current distributions, in which case the solution is unique, as we have shown in much greater detail in this paper. We believe, but have not proven, that in their three-dimensional reconstructions, the matrix that must be inverted in their algorithm will be singular. In any case, the ability of their technique to reconstruct three-dimensional current distributions has yet to be demonstrated.

V. CONCLUSIONS

Our goal in this paper was to derive an algorithm allowing us to obtain an image of a two-dimensional current distribution from measurements of the magnetic field. We have accomplished this goal, using a technique based on Fourier analysis of the data, a method commonly encountered in optical imaging. Using this technique, we can interpret magnetometer signals such as those presented in Fig. 1. Figure 12 shows the image we obtain using our analysis, as well as the current density used to calculate the data in Fig. 1. Our anal-

ysis demonstrates the key role that spatial resolution plays in determining the quality of our images. We have shown that the spatial resolution that can be obtained in our images depends on the amount of noise in our data, the size of the magnetometer pickup coil, and the distance from the current distribution to the magnetometer coil. When the coil size is too large, the inverse calculation does not have a unique solution. In many cases decreasing the current-to-coil distance improves the quality of our images more than does decreasing the magnetometer noise.

ACKNOWLEDGMENTS

We are indebted to Bascom S. Deaver and Thomas Aton for their encouragement when we began this project. This work was supported by Air Force Office of Scientific Research, Grant No. 87-0337, National Institutes of Health Grant No. 1 R01 NS 19794-5, and by grants from the American Heart Association, Tennessee affiliate, and the Whitaker Foundation. Partial support for the computing facilities was provided by the College of Arts and Sciences, Vanderbilt University.

[1]D. S. Barth, W. Sutherling, J. Engel, Jr., and J. Beatty, Science **223**, 293 (1984).

[2]B. J. Roth and J. P. Wikswo, Jr., Biophys. J. **48**, 93 (1985).

[3]B. J. Roth, Ph.D. thesis, Vanderbilt University, 1987 (unpublished).

[4]J. P. Wikswo, Jr. and B. J. Roth, Electroencephalogr. Clin. Neurophysiol. **69**, 266 (1988).

[5]J. D. Jackson, *Classical Electrodynamics* (Wiley, New York, 1975).

[6]E. Hecht and A. Zajac, *Optics* (Addison-Wesley, Reading, MA, 1979).

[7]I. S. Gradshteyn and I. M. Ryzhik, *Table of Integrals, Series and Products* (Academic, New York, 1980).

[8]A. Rosenfeld and A. C. Kak, *Digital Picture Processing* (Academic, New York, 1982); R. H. T. Bates and M. J. McDonnell, *Image Restoration and Reconstruction* (Clarendon, Oxford, 1986).

[9]J. W. Goodman, *Introduction to Fourier Optics* (McGraw-Hill, New York, 1968).

[10]A. C. Bruno, P. Costa Ribeiro, J. P. von der Weid, and O. G. Symko, J. Appl. Phys. **59**, 2584 (1986); P. Costa Ribeiro, A. C. Bruno, and C. C. Paulsen, Rev. Sci. Instrum. **58**, 1510 (1987); A. C. Bruno, A. V. Guida, and P. Costa Ribeiro, in *Biomagnetism 1987, Proceedings of the 6th International Conference on Biomagnetism,* edited by K. Atsumi, M. Kotani, S. Ueno, T. Katila, and S. J. Williamson (Tokyo Denki University Press, Tokyo, Japan, 1988), p. 454.

[11]M. Abramowitz and I. A. Stegun, *Handbook of Mathematical Functions* (U. S. Department of Commerce, Washington, D. C., 1970).

[12]G. L. Romani, S. J. Williamson, and L. Kaufman, Rev. Sci. Instrum. **53**, 1815 (1982).

[13]A. V. Oppenheim and R. W. Schafer, *Digital Signal Processing* (Prentice-Hall, Englewood Cliffs, NJ, 1975).

[14]J. R. Reitz, F. J. Milford, and R. W. Christy, *Foundations of Electromagnetic Theory* (Addison-Wesley, Reading, MA, 1980).

[15]W. J. Dallas, Appl. Opt. **24**, 4543 (1985).

[16]W. Kullmann and W. J. Dallas, IEEE Trans. Biomed. Eng. **BME-34**, 837 (1987).